Results in Materials 31 (2026) 101023

Contents lists available at ScienceDirect

Results in Materials

journal homepage: www.sciencedirect.com/journal/results-in-materials

Effect of fiber type and fiber loading on the mechanical behavior and microstructure of natural fiber reinforced polymer composites

Arum Soesanti [a,b], I Made Londen Batan [a,*], Arif Wahjudi [a], Mohammad Khoirul Effendi [a], Maulana Yusuf Izzuddin [a], Putu Suwarta [a]

[a] Department of Mechanical Engineering, Faculty of Industrial Technology and Systems Engineering, Sepuluh Nopember Institute of Technology, Surabaya, 60111, Indonesia

[b] Department of Mechanical Engineering, Faculty of Engineering, University of Surabaya, Surabaya, 60293, Indonesia

ARTICLE INFO

Keywords:
Injection molding
Polypropylene composites
Natural fiber
Tensile strength
Impact strength
Fracture morphology

ABSTRACT

Natural-fiber-reinforced polypropylene (PP) biocomposites are promising lightweight materials, but direct comparison among fiber types remains difficult because previous studies often used different materials and processing conditions. This study evaluated the effects of fiber type and loading on the tensile strength, Izod impact strength, and fracture morphology of injection-molded PP biocomposites reinforced with pineapple leaf fiber (PALF), banana fiber (BF), and coir fiber (CF). The fibers were treated with 5 wt% NaOH, ground, sieved through a 125 μm mesh, and compounded with PP and 5 wt% MAPP based on the PP/fiber blend mass. All formulations were processed under identical extrusion and injection-molding conditions at nominal fiber loadings of 10, 20, and 30 wt%. The ground particles had similar mean aspect ratios of 5.53–5.68. Processed neat PP showed tensile and impact strengths of 33.49 MPa and 1.24 kJ/m^2, respectively. PP–PALF showed the highest tensile strength of 34.91 MPa at 10 wt% and impact strength of 2.75 kJ/m^2 at 30 wt%, corresponding to numerical increases of 4.2% and 121.8% relative to processed neat PP. Two-way ANOVA showed significant effects of fiber type and loading on both properties, with a significant interaction only for tensile strength. Tensile strength decreased at higher loadings in PP–BF and PP–CF but remained relatively stable in PP–PALF, whereas impact strength generally increased. SEM revealed loading-dependent differences in matrix deformation, cavities, clustered or fiber-rich regions, exposed fibrous particles, and localized openings. Overall, PP–PALF provided the highest mean mechanical properties among the investigated systems.

1. Introduction

The need for eco-friendly and lightweight engineering materials is on the rise as a result of global environmental challenges linked to the dependence on petroleum-based substances [1,2]. Natural-fiber-reinforced polymer composites have emerged as promising alternatives in sustainable material systems. These composites offer low density, renewable reinforcement, and the potential to reduce the environmental impact and fossil-derived material content of engineering products. Recent studies on PLA-based hybrid biocomposites containing treated palm fibers and biochar have further demonstrated the potential of biodegradable matrix systems, although their performance remains strongly dependent on fiber-treatment conditions, hybrid composition, and processing route [3,4]. Consequently, they have attracted significant interest in the industrial sector, particularly within the automotive industry. The demand for lightweight materials is crucial for improving fuel efficiency and reducing emissions [5,6]. Polypropylene (PP) is widely employed as a thermoplastic matrix due to its comprehensive combination of mechanical properties, chemical resistance, ease of processing, and cost-effectiveness. Consequently, it has become a widely used matrix for natural fiber biocomposites [7].

From a manufacturing perspective, natural-fiber-reinforced thermoplastic composites can be processed using common polymer-processing techniques, especially injection molding [7]. Injection molding is widely used because it can produce complex shapes with high dimensional precision, short cycle times, and good repeatability, making it suitable for large-scale production [7,8]. Nevertheless, injection-molded natural-fiber-reinforced PP composites continue to face interfacial and processing challenges. The hydrophilic nature of lignocellulosic fibers is inherently incompatible with the hydrophobic

* Corresponding author.
E-mail address: londbatan@me.its.ac.id (I.M.L. Batan).

https://doi.org/10.1016/j.rinma.2026.101023
Received 29 May 2026; Received in revised form 30 July 2026; Accepted 5 August 2026
Available online 12 August 2026

PP matrix, which may result in weak interfacial adhesion and inefficient stress transfer [9,10].

In addition to interfacial challenges, natural fibers are susceptible to moisture uptake and thermal degradation at elevated polymer-processing temperatures. Residual moisture during melt processing may contribute to localized voids and increased porosity, which can act as stress concentrators and adversely affect composite integrity [7,11]. Furthermore, lignocellulosic fibers generally exhibit limited thermal stability and may undergo degradation at typical thermoplastic-processing temperatures. Such degradation can alter the fiber morphology and reduce its reinforcement efficiency within the composite structure [12]. These moisture- and temperature-related effects may contribute to variations in mechanical performance and reduce the reliability of natural-fiber-reinforced biocomposites, particularly in load-bearing engineering applications.

The reinforcement behavior of natural fibers is influenced by their chemical composition and structural characteristics, which affect fiber stiffness, interfacial interaction, and composite fracture behavior [13,14]. Differences in the cellulose, hemicellulose, and lignin contents may therefore contribute to variations in the mechanical properties and energy-absorption behavior of natural-fiber composites [9,13,14]. Consequently, fibers such as pineapple leaf fiber (PALF), banana fiber (BF), and coir fiber (CF) may exhibit different reinforcement responses when incorporated into polypropylene composites. Recent bio-epoxy studies using underutilized agro-waste fibers have likewise shown that increasing fiber loading can improve mechanical performance while increasing moisture sensitivity, highlighting the matrix- and formulation-dependent nature of biocomposite performance [15,16]. A scientometric analysis has also demonstrated the rapid growth and multidisciplinary development of natural-fiber-reinforced composite research [17]. However, direct comparisons among published studies remain difficult because they frequently employ different matrices, fiber treatments, compatibilizers, reinforcement dimensions, processing methods, and experimental conditions [7,13,14].

Despite growing research interest, systematic comparative studies involving different natural fibers produced under identical injection molding conditions remain limited [7]. More broadly, studies on injection-molded fiber-reinforced polypropylene have shown that processing parameters can substantially influence composite properties [18]. Therefore, differences in material composition, fiber preparation, compatibilization, and processing history can obscure the actual influence of fiber type and loading. The combined effects of natural-fiber type and loading on tensile behavior, impact resistance, and fracture morphology have not yet been sufficiently clarified under controlled and identical processing conditions. To address this gap, the present study compares PP biocomposites reinforced with PALF, BF, and CF at loadings of 10, 20, and 30 wt%. All formulations were produced using identical fiber-preparation, compatibilization, extrusion, and injection-molding conditions. This controlled approach enables a direct evaluation of the effects of fiber type and loading on the mechanical properties and fracture morphology of the resulting biocomposites.

2. Materials and methods

2.1. Materials

Polypropylene (PP) Trilene HI10HO used as the matrix was supplied by Chandra Asri Pacific Tbk. This grade was selected due to its suitability for injection molding applications. The main physical and mechanical properties of the PP grade are summarized in Table 1.

Maleic anhydride-grafted polypropylene (MAPP) was used as a compatibilizer and added at a fixed content of 5 wt%, calculated relative to the total mass of the PP/fiber blend. The natural fibers used as reinforcements were pineapple leaf fiber (PALF), banana fiber (BF), and coir fiber (CF). PALF and banana fibers were obtained from a local supplier in Subang, Indonesia, and coir fiber was sourced from a local market in Surabaya, Indonesia. These fibers were selected because they represent different lignocellulosic fiber sources and are abundantly available in Indonesia, enabling their comparative evaluation under identical material-preparation and processing conditions.

Table 1
Physical and mechanical properties of PP Trilene HI10HO.

Property	Value	Standard
Melt Flow Rate (g/10 min)	10 (230 °C/2.16 kg)	ASTM D1238
Density (g/cm^3)	0.90	ASTM D792
Tensile Yield Strength (MPa)	35	ASTM D638
Flexural Modulus (MPa)	1500	ASTM D790
Notched Izod Impact (J/m)	30	ASTM D256
Vicat Softening Temperature (°C)	152	ASTM D1525

In addition to the fiber-containing formulations, neat PP was prepared as a control material. The neat PP was subjected to the same extrusion, pelletizing, and injection-molding conditions as the biocomposite formulations. The processed neat PP provided an experimental baseline for evaluating the effect of natural fiber incorporation on the mechanical properties of the PP matrix. Neither natural fiber nor MAPP was added to the neat PP formulation.

2.2. Fiber preparation

All the fibers were subjected to an identical preparation procedure to ensure consistent processing conditions. Initially, the fibers were washed using distilled water to remove dust and surface impurities. The cleaned fibers were subsequently immersed in a 5 wt% NaOH solution for 2 h at room temperature. Previous studies have shown that the effects of chemical fiber treatment depend on the treatment agent, concentration, and duration, which can influence fiber surface characteristics, interfacial behavior, and composite performance [19–21]. Therefore, the 5 wt% NaOH treatment used in this study was applied as a common preparation condition for all three fiber types rather than as an experimentally optimized treatment.

The alkali treatment was intended to clean and modify the fiber surfaces before compounding. However, because untreated control fibers and direct chemical characterization of the treated fibers were not included in the present study, changes in hemicellulose, lignin, wax content, and surface functional groups were not quantitatively determined.

After treatment, the fibers were thoroughly rinsed with distilled water until a neutral pH was achieved to eliminate residual alkali. The washed fibers were then oven-dried at 110 °C for 24 h to minimize the moisture content before further processing. The dried fibers were ground using a high-speed grinder (WILLMAN DE200G), operating at 25,000 rpm. The ground material was subsequently sieved, and the fraction passing through a 125 μm mesh was collected for composite fabrication. The passage through the mesh was used to select a more consistent ground fraction and did not impose a strict upper limit on the particle length. The treated, ground, and sieved fibrous particles were stored in sealed containers to limit moisture uptake before compounding. The overall fiber preparation procedure is shown in Fig. 1.

The typical physical and chemical properties of PALF, banana fiber, and coir fiber reported in previous studies are summarized in Table 2 [22–24]. These literature-reported values are provided only as a general comparison of the reported compositional and mechanical characteristics of the three fiber types. They do not represent direct measurements of the treated, ground, and sieved fibrous particles used in the present study. The reported values may vary with plant source, maturity, extraction method, environmental conditions, and testing procedure.

2.3. Biocomposite fabrication

Biocomposites were fabricated using a two-step process consisting of

Fig. 1. Schematic representation of the fiber preparation process, including alkali treatment, rinsing, drying, grinding, and sieving.

Table 2
Typical physical and chemical properties of untreated PALF, banana fiber, and coir fiber [22–24].

Property	PALF	Banana Fiber	Coir Fiber
Density (g/cm^3)	1.07–1.50	1.35	1.10–1.50
Cellulose (%)	70–82	43.46–64	32–50
Hemicellulose (%)	5–12.7	10–38.54	0.15–15
Lignin (%)	5–12	5–9	30–46
Tensile Strength (MPa)	413–1627	54–754	105–593

melt compounding followed by injection molding. Prior to processing, polypropylene (PP), maleic anhydride-grafted polypropylene (MAPP), and the prepared natural fibers were dried to minimize their moisture content and prevent defects during processing. To enhance the interfacial bonding between the hydrophilic fibers and hydrophobic PP matrix, MAPP was added at a fixed content of 5 wt%, based on the total mass of the PP/fiber blend.

In the first stage, PP and natural fibers with different loadings (10, 20, and 30 wt%) were compounded using a conventional single-screw extruder with a screw diameter of 26 mm and L/D ratio of approximately 23. The extrusion process was conducted at a barrel temperature of 180 °C to melt the PP matrix and enable compounding with the prepared fibrous particles. The screw speed was controlled using an inverter and maintained at a constant setting throughout the process to ensure stable material flow and consistent processing conditions. The extrudate obtained from the extrusion process was subsequently cooled and pelletized into granules.

In the second stage, the composite pellets were processed using an injection molding machine (MA900 II S) to produce standard test specimens. The barrel temperature was set with a temperature profile ranging from 160 to 200 °C, and the nozzle temperature was maintained at 175 °C. The injection and holding pressures were set at 55 and 30 bar, respectively, with injection and holding times of 7 s and 2 s, respectively. All processing parameters were kept constant throughout the experiments to ensure consistent and reliable comparisons between different fiber types and loadings.

The overall fabrication route of the biocomposites is schematically illustrated in Fig. 2, which highlights the sequential stages of extrusion, pelletizing, and injection molding.

Based on this processing approach, the experimental design and composition of the biocomposites are summarized in Table 3.

MAPP content was calculated relative to the total mass of the PP/fiber blend and was added separately. A total of nine fiber-containing biocomposite formulations and one neat PP control were prepared to systematically evaluate the effects of fiber type and fiber loading under identical processing conditions.

3. Characterization and testing

3.1. Fiber dimensional characterization

Following grinding and sieving, the dimensions of the processed fibers were characterized using a trinocular optical microscope (T490B, AmScope, USA) equipped with a 14 MP CMOS digital camera (MU1403, AmScope, USA). Optical micrographs were calibrated before measurement. For each fiber type, 100 randomly selected particles were

Table 3
Experimental design and compositions of the neat PP control and biocomposite formulations.

Sample Code	Fiber Type	Fiber Loading (wt %)	MAPP addition (wt% of PP/fiber blend)
PP	None	0	0
BF10	Banana fiber	10	5
BF20	Banana fiber	20	5
BF30	Banana fiber	30	5
PF10	PALF	10	5
PF20	PALF	20	5
PF30	PALF	30	5
CF10	Coir fiber	10	5
CF20	Coir fiber	20	5
CF30	Coir fiber	30	5

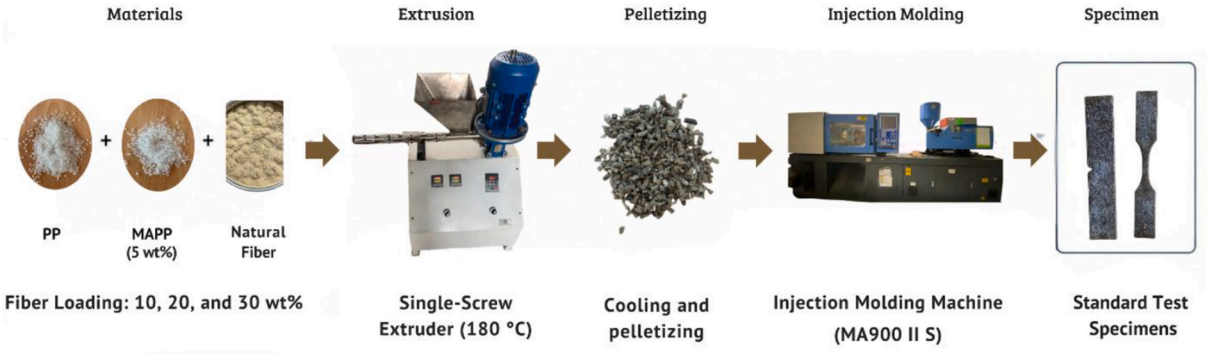

Fig. 2. Biocomposite fabrication process for standard test specimens.

measured. The longest projected dimension was defined as the particle length (L), whereas the transverse dimension perpendicular to the major axis was defined as the particle width (D). The aspect ratio was calculated as L/D. The results were expressed as the mean ± standard deviation and range.

3.2. Mechanical properties

3.2.1. Tensile test

The tensile properties of the biocomposites were evaluated in accordance with ASTM D638-03 using Type V specimens and a universal testing machine (SALT ST-1001, Solid Mechanics Laboratory, Department of Mechanical Engineering, Institut Teknologi Sepuluh Nopember). The specimens were prepared by injection molding into a standard dumbbell shape.

The tests were conducted at room temperature at a constant crosshead speed of 3 mm/min. Five specimens were tested for each formulation. The results are presented as mean values, while the error bars in Fig. 3a represent the standard error (SE). Tensile strength was determined from the stress–strain data. Five processed neat PP specimens were also tested under identical conditions to provide an experimental baseline for comparison with the tensile properties of the biocomposite formulations.

3.2.2. Impact test

The impact properties of the biocomposites were evaluated in accordance with ASTM D256-04 using the Izod impact test method. The specimens were prepared by injection molding with a standard notch configuration.

The tests were performed using an Izod impact tester (TESTONE TO-

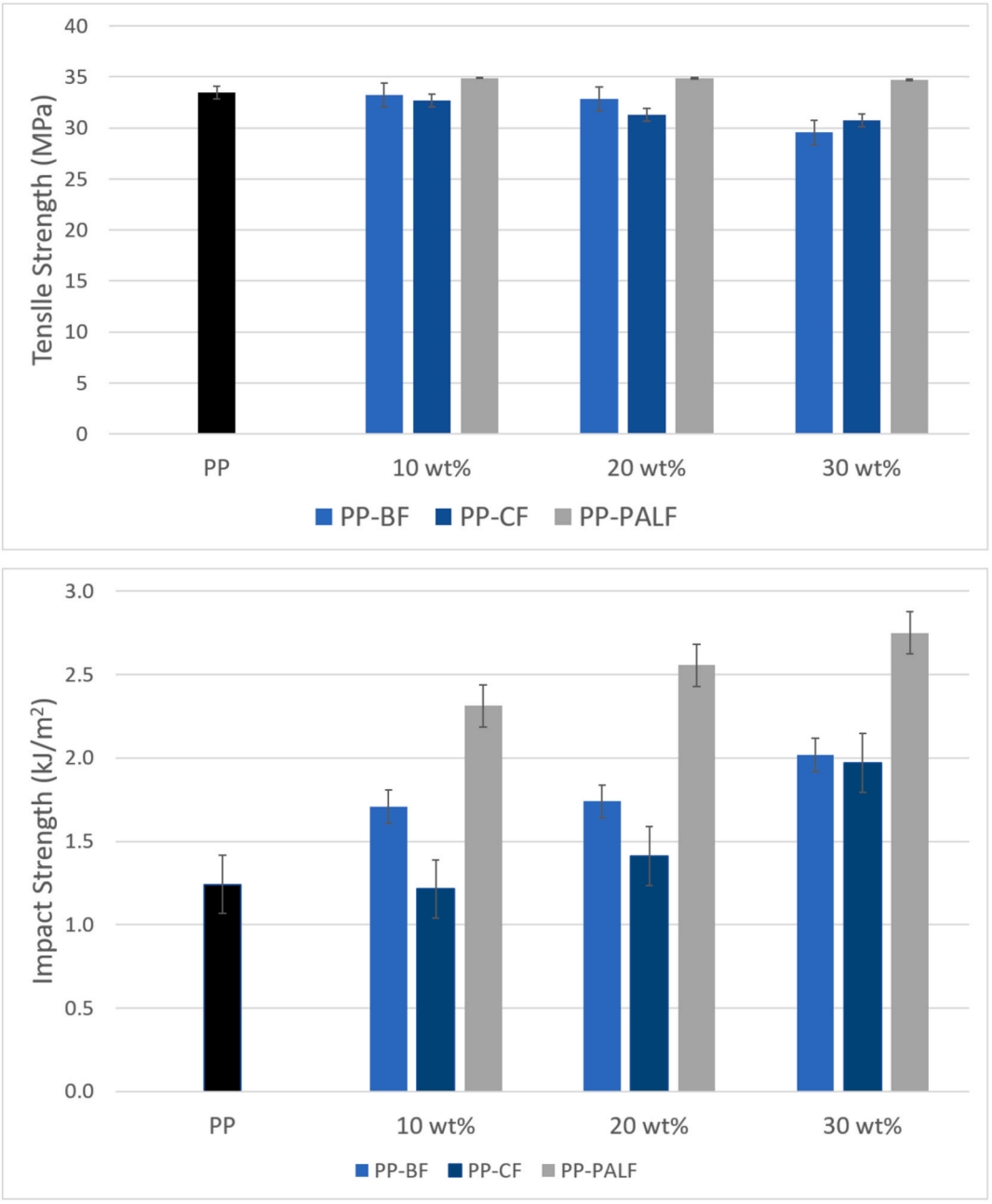

Fig. 3. Tensile and impact strengths of processed neat PP and natural-fiber-reinforced PP biocomposites: (a) tensile strength and (b) impact strength at different fiber loadings. Bars represent mean values, and error bars represent the standard error (SE).

700D) at room temperature. Five specimens were tested for each formulation, including the processed neat PP control. The results are presented as mean values, while the error bars in Fig. 3b represent the standard error (SE). The impact strength was calculated by dividing the absorbed fracture energy by the cross-sectional area of the specimen at the notch and was expressed in kJ/m^2.

3.3. Morphological analysis

The morphological characteristics of the fractured surfaces of the biocomposites were examined using scanning electron microscopy (SEM) (Hitachi FlexSEM 1000 II). Prior to observation, the fractured specimens were sputter-coated with a thin layer of gold to enhance surface conductivity. The micrographs were qualitatively examined to identify visible fracture features, including matrix deformation and tearing, cavities, exposed fibrous particles, clustered or fiber-rich regions, localized openings, and pull-out-like traces.

3.4. Statistical analysis

Tensile and Izod impact strength data were analyzed separately using two-way analysis of variance (ANOVA). Fiber type (BF, CF, and PALF) and fiber loading (10, 20, and 30 wt%) were treated as fixed factors, and the interaction between these factors was included in the statistical model. Statistical significance was evaluated at $p < 0.05$. All statistical analyses were performed using Minitab 21. Processed neat PP was excluded from the two-way ANOVA because it was not part of the fiber type × fiber loading factorial design.

4. Results and discussion

4.1. Dimensional characteristics of the ground fiber particles

The dimensions of the ground and sieved fiber particles were measured to determine whether the preparation procedure retained an elongated fibrous morphology or produced predominantly particulate material. The dimensional characteristics of the processed PALF, banana fiber, and coir fiber particles are summarized in Table 4.

PALF exhibited the highest mean particle length of 110.14 ± 37.91 μm, followed by banana fiber at 91.17 ± 21.74 μm and coir fiber at 81.46 ± 15.47 μm. However, the mean aspect ratios of the three fiber types were relatively similar, ranging from 5.53 to 5.68. These results indicate that high-speed grinding and sieving produced low-aspect-ratio fibrous particles rather than intact long fibers. The particles retained an elongated morphology but would not be expected to form a continuous long-fiber reinforcement network. Therefore, their mechanical contribution is interpreted in terms of the combined effects of particle geometry, dispersion, matrix continuity, and interfacial interaction. Although the particles retained an elongated morphology, the measured aspect ratio alone cannot establish whether they exceeded the critical aspect ratio because the tensile strength of the treated particles and the fiber–matrix interfacial shear strength were not directly measured [25].

Table 4
Dimensional characteristics of the ground and sieved natural-fiber particles.

Fiber type	n	Length, L (μm)	Width, D (μm)	Aspect ratio, L/D
PALF	100	110.14 ± 37.91 (40.21–193.71)	20.95 ± 8.48 (7.40–46.34)	5.57 ± 1.54 (3.23–9.74)
Banana fiber	100	91.17 ± 21.74 (50.21–166.20)	16.48 ± 4.15 (7.53–27.17)	5.68 ± 1.22 (3.85–8.54)
Coir fiber	100	81.46 ± 15.47 (44.94–121.63)	15.26 ± 3.42 (8.55–24.48)	5.53 ± 1.32 (3.10–8.68)

Values are presented as mean ± standard deviation; minimum–maximum values are shown in parentheses.

However, the relatively similar and low aspect ratios of the three particle types did not produce an identical tensile-strength trend across all composite systems. The reductions at higher particle loadings were more pronounced in the PP–BF and PP–CF systems, whereas the PP–PALF system maintained relatively stable mean tensile strength across the investigated loadings. Therefore, the tensile response cannot be attributed solely to the low aspect ratio or particulate-like behavior of the ground particles. The differences among the three systems likely resulted from the combined effects of particle dimensions, particle-specific characteristics, dispersion, matrix continuity, and interfacial interaction.

4.2. Tensile strength

Fig. 3a compares the tensile strengths of the processed neat PP control and the natural-fiber-reinforced PP biocomposites. The processed neat PP exhibited a mean tensile strength of 33.49 MPa. Among the fiber-containing formulations, PP–PALF at 10 wt% showed the highest mean tensile strength of 34.91 MPa, which was numerically 4.2% higher than that of the processed neat PP. In contrast, several PP–BF and PP–CF formulations exhibited tensile strengths comparable to or lower than that of the neat PP control, particularly at higher fiber loadings. These results indicate that the effect of natural fiber incorporation on tensile performance depended on both fiber type and fiber loading, rather than producing a uniform improvement across all formulations.

The two-way ANOVA results presented in Table 5 showed that fiber type had a significant effect on tensile strength ($F = 23.885$, $p < 0.0001$). Fiber loading also significantly affected tensile strength ($F = 7.416$, $p = 0.0020$). Moreover, the interaction between fiber type and fiber loading was statistically significant ($F = 2.638$, $p = 0.0497$), although the interaction effect was close to the significance threshold. These results indicate that the effect of increasing fiber loading on tensile strength depended on the type of natural fiber. The relatively stable tensile strength of the PP–PALF system, compared with the more pronounced reductions observed in PP–BF and PP–CF at higher loadings, is consistent with this interaction effect.

However, the tensile behavior of natural fiber composites is not solely governed by the inherent properties of reinforcing fibers. The reinforcement efficiency also depends on the quality of the fiber–matrix interface, which influences the stress transfer during tensile loading. Previous studies have shown that fiber surface characteristics, treatment conditions, and compatibilization play important roles in determining the interfacial adhesion and tensile performance of natural fiber-reinforced polymer composites [26,27].

Under the same extrusion and injection-molding conditions, PP–PALF maintained relatively stable mean tensile strength across the investigated loadings, whereas PP–BF and PP–CF exhibited larger decreases at higher particle loadings. This behavior suggests that the reinforcement efficiency depends not only on the fiber loading but also on the interaction between the fiber distribution and matrix continuity. At moderate loading, the fibrous particles may contribute to stress

Table 5
Two-way ANOVA results for the tensile strength of the biocomposite formulations.

Source	DF	Adjusted SS	Adjusted MS	F-value	p-value
Fiber type	2	96.591	48.296	23.885	<0.0001
Fiber loading	2	29.989	14.994	7.416	0.0020
Fiber type × fiber loading	4	21.339	5.335	2.638	0.0497
Error	36	72.792	2.022	—	—
Total	44	220.711	—	—	—

Note: Statistically significant effects are indicated by $p < 0.05$.

transfer and improve load-bearing capability. However, increasing the fiber content may also increase the likelihood of fiber agglomeration and reduce the ability of molten polypropylene to adequately wet the fiber surface, resulting in weaker interfacial bonding and lower reinforcement efficiency [28]. A similar loading-related tendency was reported by Nampitch et al. [29], who found that excessive bagasse-fiber content increased fiber agglomeration and matrix viscosity in PLA/natural-rubber composite foams. However, direct comparison is limited by differences in matrix system, foam structure, and processing route. In contrast, Singh et al. [30] reported the highest tensile strength at 30 vol% fiber loading in compression-molded jute/PLA composites under their selected curing conditions. This contrasting trend highlights the dependence of reinforcement efficiency on the matrix, fiber architecture, and processing conditions.

It should also be noted that the values presented in Table 2 represent typical literature data for untreated fibers. The actual properties of the treated fibers used in this study may vary depending on the plant source, extraction method, and treatment effectiveness. Therefore, the correlations discussed here should be interpreted as general supporting trends rather than direct property equivalences. Direct chemical characterization of the treated and ground particles would provide a more precise understanding of the relationship between alkali-induced chemical changes and composite performance.

The processing conditions may also contribute to the tensile response. During injection molding, shear flow influences the fiber orientation, dispersion, and local distribution within the polypropylene matrix, which subsequently affects the stress transfer efficiency and tensile behavior of the composite. Previous studies have emphasized that fiber orientation and dispersion play important roles in determining the tensile response of thermoplastic composites containing low-aspect-ratio fibrous particles, particularly when combined with interfacial bonding effects [25]. The relatively consistent tensile behavior observed in the PALF biocomposites may reflect the combined effects of the fiber characteristics and the microstructure formed during processing.

Overall, the results demonstrate that the tensile performance of injection-molded biocomposites is governed by the combined influence of fiber type, fiber loading, and fiber–matrix interaction. Although an increase in fiber loading can enhance the reinforcement content, an excessively high fiber concentration may reduce the tensile performance. This decline may be associated with inadequate particle dispersion, reduced matrix continuity, and localized interfacial discontinuities. Therefore, both particle-specific characteristics and particle–matrix interactions must be considered in the development of natural-fiber-reinforced PP biocomposites.

4.3. Impact strength

Fig. 3b compares the Izod impact strengths of the processed neat PP control and the natural-fiber-reinforced PP biocomposites. The processed neat PP exhibited a mean impact strength of 1.24 kJ/m^2. Most fiber-containing formulations showed numerically higher mean impact strengths than the processed neat PP control, except for PP–CF at 10 wt %, which showed a similar mean value. Among the biocomposite formulations, PP–PALF at 30 wt% showed the highest mean impact strength of 2.75 kJ/m^2, representing a numerical increase of approximately 121.8% relative to processed neat PP. These results indicate that the incorporation of the ground natural-fiber particles influenced the impact-energy absorption of the PP matrix, although the magnitude of the response depended on both particle type and loading.

As shown in Table 6, fiber type had a significant effect on Izod impact strength ($F = 100.443$, $p < 0.0001$). Fiber loading also produced a significant effect ($F = 23.758$, $p < 0.0001$). However, the interaction between fiber type and fiber loading was not statistically significant ($F = 2.214$, $p = 0.0869$). These findings indicate that both the selected fiber and the amount of fiber incorporated influenced the impact response. However, at the 5% significance level, the pattern of the loading effect was not sufficiently different among the three fiber systems to establish a significant interaction.

Table 6
Two-way ANOVA results for the Izod impact strength of the biocomposite formulations.

Source	DF	Adjusted SS	Adjusted MS	F-value	p-value
Fiber type	2	8.253	4.127	100.443	<0.0001
Fiber loading	2	1.952	0.976	23.758	<0.0001
Fiber type × fiber loading	4	0.364	0.091	2.214	0.0869
Error	36	1.479	0.041	—	—
Total	44	12.049	—	—	—

Note: Statistically significant effects are indicated by $p < 0.05$.

Literature-reported properties of untreated fibers, as summarized in Table 2, suggest that PALF may possess relatively high cellulose content and tensile strength. However, these values cannot be directly assigned to the treated and ground particles used in the present study because alkali treatment, plant source, and high-speed grinding may alter their chemical and structural characteristics. Although crystalline cellulose content and microfibril angle may influence intrinsic fiber stiffness [31], the comparatively high mean impact-strength values of the PP–PALF formulations cannot be attributed solely to these structural characteristics. The observed response likely resulted from the combined effects of particle dimensions, particle distribution, interfacial interaction, matrix continuity, and processing-induced microstructure. Khuntia and Biswas [32] also demonstrated that coir loading influenced the mechanical and viscoelastic responses of coir-reinforced PP composites. However, their processing route and investigated properties differed from those of the present study. Under identical extrusion and injection-molding conditions, the PP–PALF formulations generally exhibited higher mean impact-strength values than the corresponding PP–BF and PP–CF formulations.

The impact behavior was also influenced by fiber loading, with variations observed depending on the type of fiber used. In general, increasing the fiber loading tended to improve the impact strength, indicating that a higher reinforcement fraction may contribute to greater energy absorption during impact loading [33]. When the fiber dispersion and fiber-matrix interaction are well maintained, the fibrous particles may participate more effectively in transferring and dissipating impact energy. This increases the resistance to impact-induced damage [34]. However, the effect of fiber loading is not always linear. Although increasing the fiber content may enhance the reinforcement contribution, excessive loading can reduce the impact performance when fiber agglomeration, non-uniform distribution, or inadequate interfacial interaction limit the reinforcement efficiency. Under such conditions, localized stress concentrations and less effective energy dissipation may promote earlier damage initiation and reduce the resistance of the composite to fracturing [35]. Sultana et al. [36] demonstrated that fiber architecture and surface treatment can substantially improve the impact performance of short-jute-fiber-reinforced PP composites. This finding further indicates that impact strength depends not only on fiber content but also on reinforcement architecture and processing.

The processing conditions also contributed to the observed impact response. During injection molding, the flow-induced fiber orientation and local fiber distribution influence the microstructure of the polypropylene matrix. This microstructure subsequently affects the fracture and impact behavior. Previous studies have highlighted that the processing–morphology relationship plays an important role in determining the mechanical and fracture behavior of injection-molded natural-fiber composites [37]. In this study, the PALF biocomposite exhibited a relatively high impact strength. This behavior may reflect the combined influence of particle-specific characteristics and the microstructure developed during processing.

Overall, the results indicate that the impact performance of injection-molded polypropylene biocomposites was influenced by the combined effects of particle type, particle loading, particle–matrix interaction, and processing-induced microstructure. Although increasing the fiber content has the potential to enhance the impact resistance, the reinforcement effectiveness depends on good fiber dispersion and adequate interfacial interactions within the composite structure. Under the processing conditions applied in this study, the PP–PALF formulations generally exhibited the highest mean impact-strength values among the investigated fiber systems. These findings emphasize that fiber selection and processing-induced microstructure are important considerations in the development of injection-molded polypropylene biocomposites for engineering applications.

4.4. Morphological characteristics

The tensile-fracture morphologies of the PP–PALF, PP–BF, and PP–CF composites are presented in Figs. 4–6, respectively. All composite systems were produced under identical extrusion and injection-molding conditions. Distinct differences were observed in matrix deformation and tearing, cavity formation, clustered or fiber-rich regions, exposed fibrous particles, and localized openings. The PP–BF composites exhibited increasingly prominent clustered regions at higher fiber loadings, whereas the PP–PALF composites retained visible matrix involvement accompanied by localized cavities and fibrous regions. The PP–CF composites showed more distinct exposed fibrous particles, localized interfacial openings, cavities, and pull-out-like features, particularly at 20 and 30 wt%. These observations indicate that fiber type and loading were associated with differences in the tensile-fracture morphology of the biocomposites.

In the PP–PALF system, the tensile-fracture morphology changed with increasing fiber loading. At 10 wt%, the fracture surface remained relatively matrix-dominated, with visible matrix tearing and deformation, localized cavities, and an exposed fibrous particle. A localized interfacial opening was also observed along the boundary of the exposed particle. At 20 wt%, an exposed fibrous particle and localized cavity were evident, accompanied by an interfacial opening and matrix tearing in the surrounding region. At 30 wt%, the fracture surface exhibited more pronounced matrix tearing, a localized cavity, and a fiber-rich region. These observations indicate that increasing the PALF loading altered the local balance between matrix continuity and fibrous regions, while matrix tearing remained involved in the tensile-fracture process. Shibly et al. [38] similarly reported that fiber treatment and the resulting fiber–matrix morphology influenced the mechanical response of a natural-fiber-reinforced PP composite.

In the PP–BF system, the tensile-fracture morphology became progressively more heterogeneous with increasing fiber loading. At 10 wt%, the fracture surface remained predominantly matrix-dominated, with visible matrix tearing and deformation accompanied by a localized cavity and opening. At 20 wt%, a prominent clustered region was observed, together with a localized cavity, opening, and matrix tearing. The clustered region locally interrupted the continuity of the surrounding matrix. At 30 wt%, another prominent clustered region and a larger localized opening were evident, accompanied by matrix tearing and deformation. These features suggest a less uniform local distribution of the ground banana-fiber particles and the development of local discontinuities at higher fiber loadings. Morphological changes associated with reinforcement distribution and interfacial modification have also

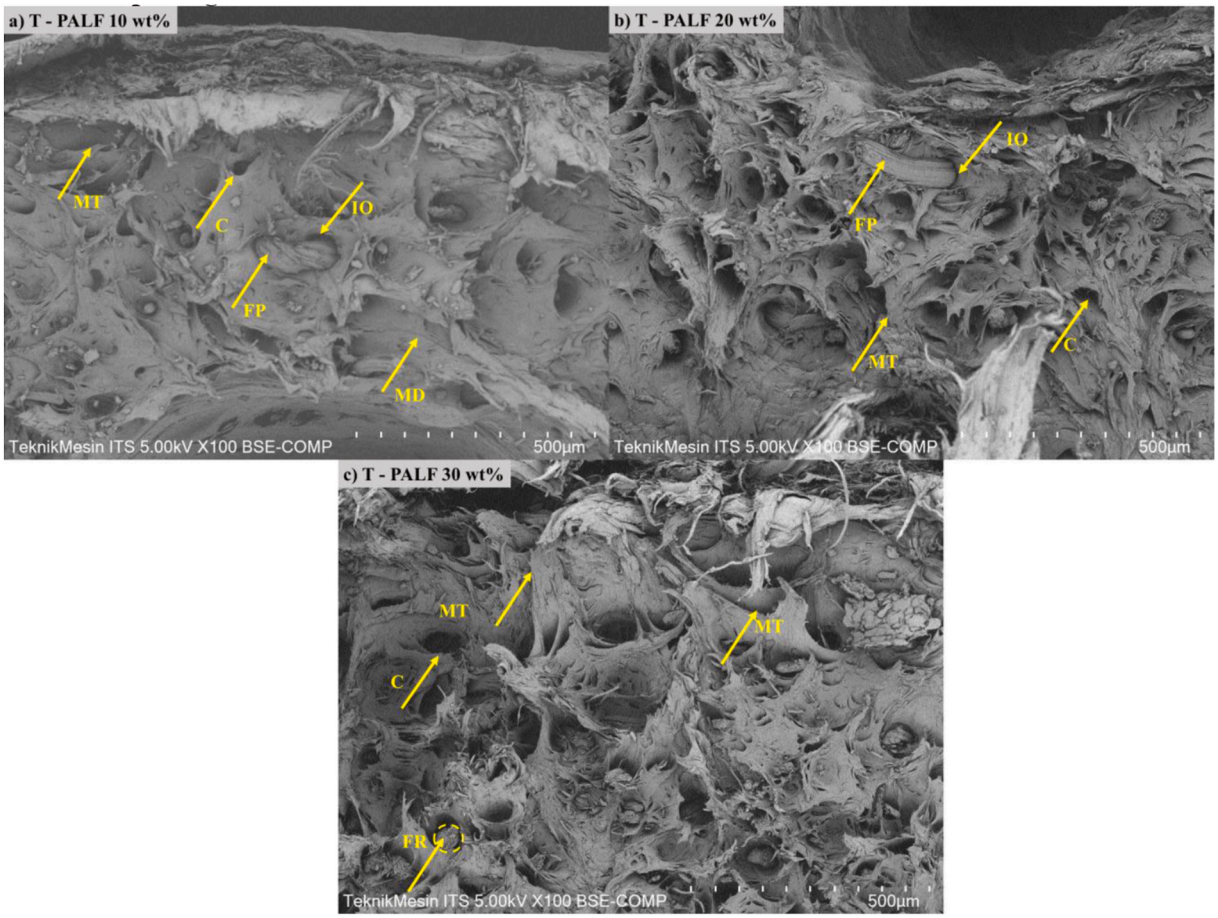

Fig. 4. SEM micrographs of the tensile-fracture surfaces of PP–PALF composites at (a) 10 wt%, (b) 20 wt%, and (c) 30 wt% fiber loading. MT: matrix tearing; C: cavity; FP: exposed fibrous particle; IO: localized interfacial opening; MD: matrix deformation; FR: fiber-rich region.

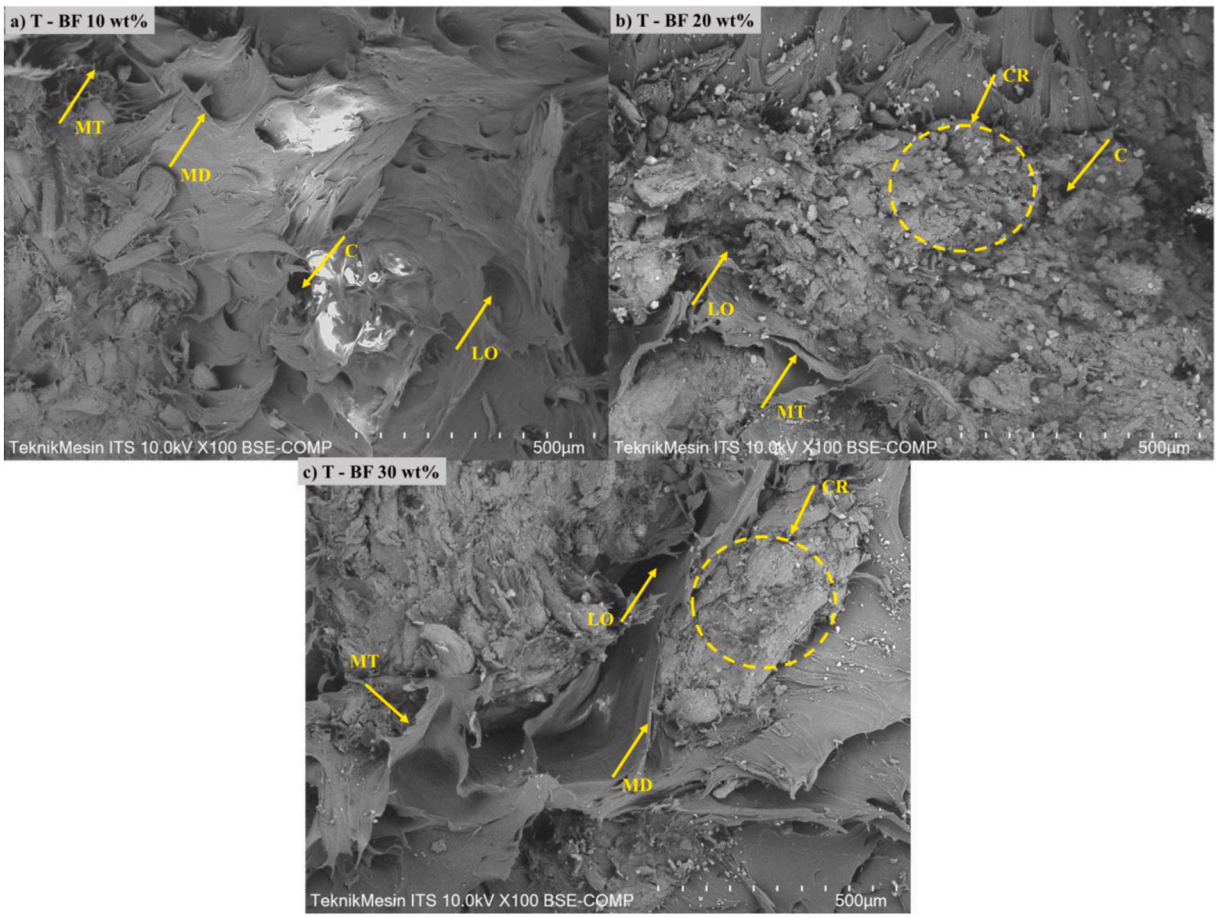

Fig. 5. SEM micrographs of the tensile-fracture surfaces of PP–BF composites at fiber loadings of (a) 10 wt%, (b) 20 wt%, and (c) 30 wt%. MT: matrix tearing; MD: matrix deformation; C: cavity; LO: localized opening; CR: clustered region.

been reported in wheat-straw/recycled-PP nanocomposites [39]. However, that system included modified montmorillonite and different treatment conditions.

In the PP–CF system, the tensile-fracture morphology changed with increasing fiber loading and showed increasingly distinct particle- and interface-related features. At 10 wt%, the fracture surface remained relatively matrix-dominated, with visible matrix deformation and tearing, a small localized cavity, and a large cavity-like depression. At 20 wt%, an exposed fibrous particle and a localized interfacial opening were clearly visible, accompanied by a cavity, a larger localized opening, and matrix tearing. At 30 wt%, the fracture surface exhibited an exposed fibrous particle, a localized interfacial opening, matrix tearing, and a localized cavity. An elongated opening with a relatively smooth internal surface was identified as a pull-out-like trace, suggesting the possible removal of a fibrous particle during tensile fracture. These features indicate that particle–matrix interactions and localized discontinuities became more evident in the PP–CF system at higher fiber loadings.

Overall, the annotated SEM micrographs indicate that the tensile-fracture morphology of the investigated biocomposites was influenced by fiber type and loading. Differences in matrix continuity, matrix deformation and tearing, cavity formation, clustered or fiber-rich regions, exposed fibrous particles, localized interfacial openings, and pull-out-like features were observed among the PP–PALF, PP–BF, and PP–CF systems. At higher fiber loadings, clustered regions and localized openings became more prominent in PP–BF, whereas exposed fibrous particles and interface-related features became more evident in PP–CF. PP–PALF retained visible matrix involvement across the investigated loadings, although localized cavities and a fiber-rich region were also observed. These morphological features may influence local stress distribution and stress-transfer efficiency during tensile loading. These interpretations are consistent with broader reviews of biomass-particulate-reinforced thermoplastics, which identify particle distribution, interfacial quality, and matrix continuity as important determinants of mechanical behavior [40].

The impact-fracture morphologies of the PP–PALF, PP–BF, and PP–CF composites are presented in Figs. 7–9, respectively. All composite systems were produced under identical extrusion and injection-molding conditions. The annotated SEM micrographs show differences in localized cavities and openings, relatively matrix-dominated regions, exposed fibrous particles, rough or clustered regions, matrix deformation, and large depressions. These observations indicate that fiber type and loading influenced the local development of the fracture surfaces during impact failure. However, because the PP–PALF micrographs were obtained at 30× magnification, whereas the PP–BF and PP–CF micrographs were obtained at 50×, comparisons among the three systems are qualitative and are based primarily on the types and distributions of visible features rather than their apparent dimensions. The impact-fracture morphology is therefore interpreted as resulting from several interacting microstructural features rather than from a single fracture mechanism [41].

In the PP–PALF system, the impact-fracture morphology changed with increasing fiber loading. At 10 wt%, several localized cavities were visible, including a cluster of closely spaced cavities and an elongated cavity, together with an exposed fibrous particle. At 20 wt%, the fracture surface contained a relatively compact region and a rough region, accompanied by an isolated cavity and an exposed fibrous particle. The presence of a relatively compact region suggests that matrix continuity

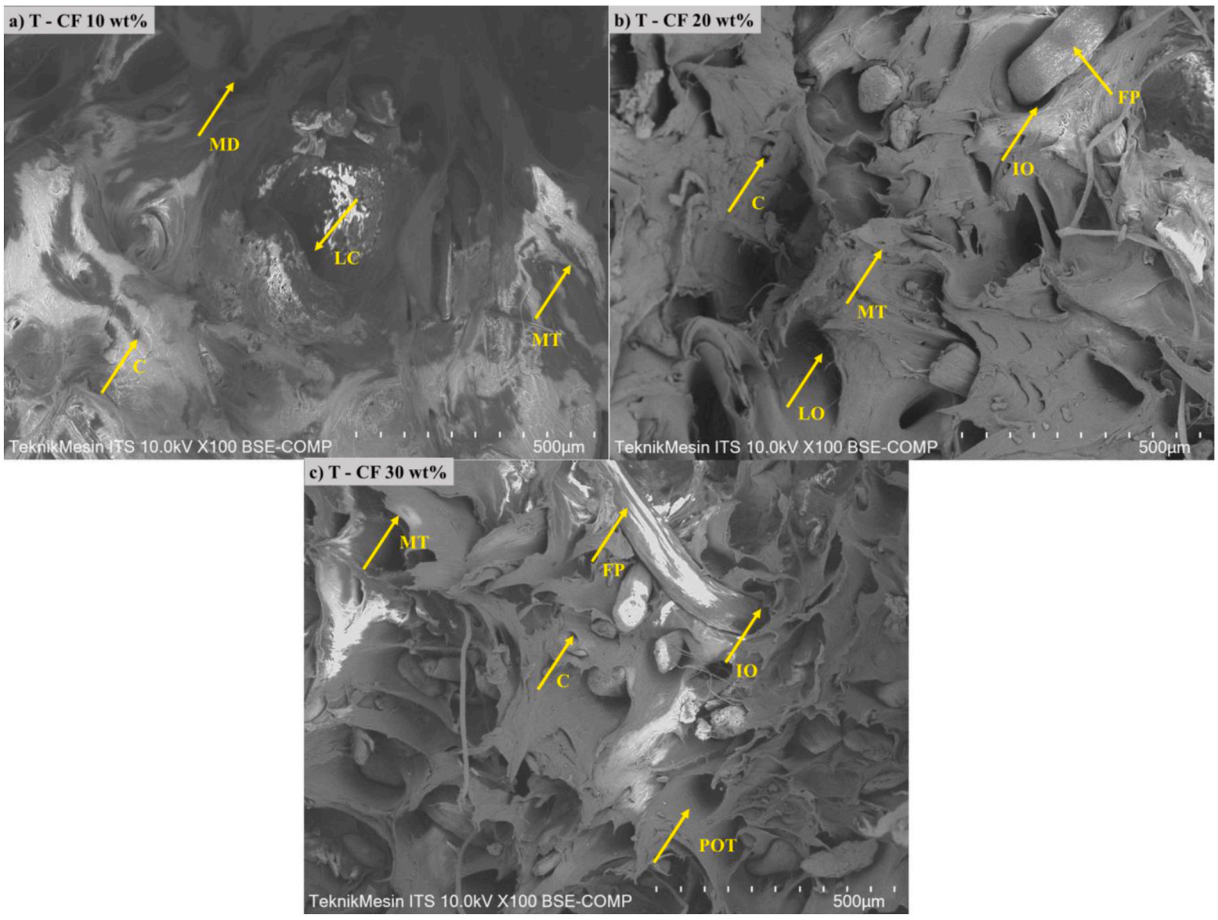

Fig. 6. SEM micrographs of the tensile-fracture surfaces of PP–CF composites at fiber loadings of (a) 10 wt%, (b) 20 wt%, and (c) 30 wt%. MD: matrix deformation; LC: large cavity-like depression; MT: matrix tearing; C: cavity; FP: exposed fibrous particle; IO: localized interfacial opening; LO: localized opening; POT: pull-out-like trace.

was locally retained, although the fracture surface was not entirely homogeneous. At 30 wt%, a large cavity, a localized opening, matrix deformation, a smaller cavity, and an exposed fibrous particle were observed. These features indicate that the local morphology became more complex at the highest PALF loading, with matrix deformation occurring around prominent surface discontinuities. Overall, the PP–PALF system exhibited loading-dependent changes from clustered and elongated cavities at 10 wt%, to a locally more compact morphology at 20 wt%, and to a large cavity and localized matrix deformation at 30 wt%. Loading-dependent changes in fracture morphology were also reported by Lalaymia et al. [42] for agave-fiber-reinforced bio-epoxy composites. However, direct comparison should be made cautiously because of differences in matrix chemistry, fiber geometry, and manufacturing process.

In the PP–BF system, the impact-fracture morphology also varied with fiber loading, although the changes were not strictly monotonic. At 10 wt%, the fracture surface contained a relatively matrix-dominated region, an isolated cavity, and an exposed fibrous particle. At 20 wt%, a distinct clustered region and a localized cavity were observed, while a relatively matrix-dominated region remained visible in another part of the fracture surface. At 30 wt%, several exposed fibrous particles and a localized cavity were visible, together with a relatively matrix-dominated region. These observations indicate that increasing the banana-fiber loading altered the local distribution of the exposed particles and clustered features, but did not produce a uniform or continuously increasing loss of matrix-dominated regions. The clustered region observed at 20 wt% and the more visible exposed fibrous particles at 30 wt% demonstrate that the local impact-fracture morphology depended on the spatial distribution of the ground banana-fiber particles. Abdullah et al. [43] also reported that filler distribution and fiber–matrix morphology influenced the properties of banana- and bamboo-filled epoxy composites. However, direct comparison is limited by differences in matrix type and fabrication process.

In the PP–CF system, the impact-fracture surface at 10 wt% was characterized primarily by a relatively matrix-dominated region and an isolated cavity. At 20 wt%, an exposed fibrous particle, a localized opening, and a localized cavity became more apparent. At 30 wt%, the fracture surface contained an exposed fibrous particle, a localized cavity, and a large depression. These observations indicate that particle- and opening-related features became more visually prominent at the intermediate and higher coir-fiber loadings. However, the origin of the large depression and localized openings cannot be determined solely from the SEM images; they may have developed during impact fracture or may represent pre-existing local discontinuities. Therefore, these features are described morphologically without assigning them conclusively to void formation, interfacial debonding, or particle pull-out. Interfacial voids and fiber pull-out features have also been reported in recycled-LDPE hybrid composites reinforced with natural fibers and paper-pulp fillers [44]. However, the hybrid reinforcement system and compression-molding process differ from those used in the present study.

Overall, the annotated SEM micrographs indicate that the impact-fracture morphology of the investigated biocomposites was influenced by fiber type and loading. The PP–PALF system exhibited cavity clusters and an elongated cavity at 10 wt%, a locally compact region at 20 wt%, and a large cavity accompanied by matrix deformation at 30 wt%. In the

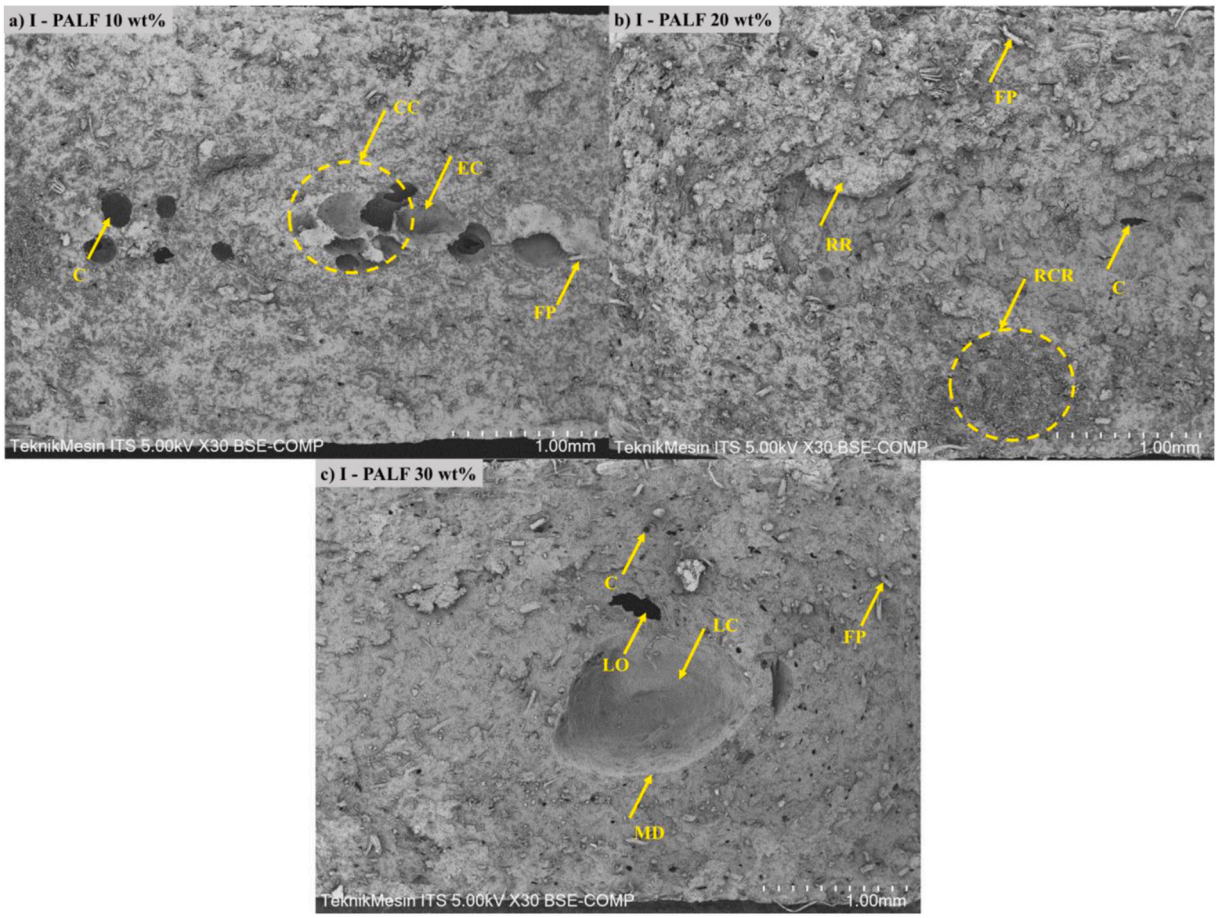

Fig. 7. SEM micrographs of the impact-fracture surfaces of PP–PALF composites at (a) 10 wt%, (b) 20 wt%, and (c) 30 wt% fiber loading. C: cavity; CC: cavity cluster; EC: elongated cavity; FP: exposed fibrous particle; RR: rough region; RCR: relatively compact region; LO: localized opening; LC: large cavity; MD: matrix deformation.

PP–BF system, matrix-dominated regions remained visible at all loadings, while a clustered region was most apparent at 20 wt% and exposed fibrous particles were more visible at 30 wt%. The PP–CF system changed from a predominantly matrix-dominated surface at 10 wt% to more distinct exposed particles, localized openings, cavities, and a large depression at 20 and 30 wt%. These features may influence local crack propagation and energy dissipation during impact loading. Nevertheless, SEM observations alone cannot quantitatively determine the contribution of each feature to the measured impact strength. The impact response is therefore interpreted as resulting from the combined effects of particle-specific characteristics, local particle distribution, matrix continuity, interfacial interaction, and processing-induced microstructure. Kyatanavar et al. [45] similarly combined mechanical testing and SEM fracture analysis to evaluate the effects of natural-fiber and bio-waste-filler composition on composite performance. Their use of ANN further demonstrated the potential of composition-based predictive approaches, although their hybrid phenol-formaldehyde system differs substantially from the injection-molded PP composites investigated here.

Although MAPP was added at a fixed content of 5 wt% based on the PP/fiber blend mass, its relative availability decreased as the nominal fiber loading increased. The nominal MAPP-to-fiber mass ratio decreased from 0.50 at 10 wt% fiber loading to 0.25 at 20 wt% and approximately 0.17 at 30 wt%. The increasing amount of ground fiber particles likely increased the interfacial area that required wetting by the PP matrix and compatibilization by MAPP. In addition, the higher solid fraction may have increased the melt viscosity, restricted matrix penetration between closely spaced particles, and promoted localized fiber agglomeration [28,40]. Consequently, the fixed MAPP content may not have provided uniform interfacial modification throughout the highly filled composite, particularly at 30 wt% fiber loading, which may have contributed to localized interfacial openings and reduced matrix continuity.

Nevertheless, SEM fracture morphology alone cannot confirm whether the selected MAPP addition level was chemically insufficient. Compatibilization efficiency also depends on the maleic anhydride grafting level, fiber surface chemistry, particle size and aspect ratio, residual moisture, fiber dispersion, and the shear and residence-time history during processing [26]. Because these parameters were not directly quantified, the interfacial features observed at 30 wt% are interpreted as indicating a possible limitation of the fixed compatibilizer content and processing conditions rather than definitive evidence of MAPP failure.

4.5. *Limitations of the study*

The processed neat PP control did not contain MAPP. Therefore, comparisons with the fiber-containing formulations represent the combined effects of fiber incorporation and MAPP addition, and the independent contribution of MAPP could not be determined.

This study has several limitations that should be considered when interpreting the mechanical and morphological results. Direct chemical characterization of the treated and ground fiber particles using FTIR was not performed, and untreated fibers were not characterized using the same analytical procedure. Therefore, changes in chemical composition and functional groups resulting from the alkali treatment could not be quantified. Accordingly, the literature values presented for untreated fibers in Table 2 are used only as general background information and

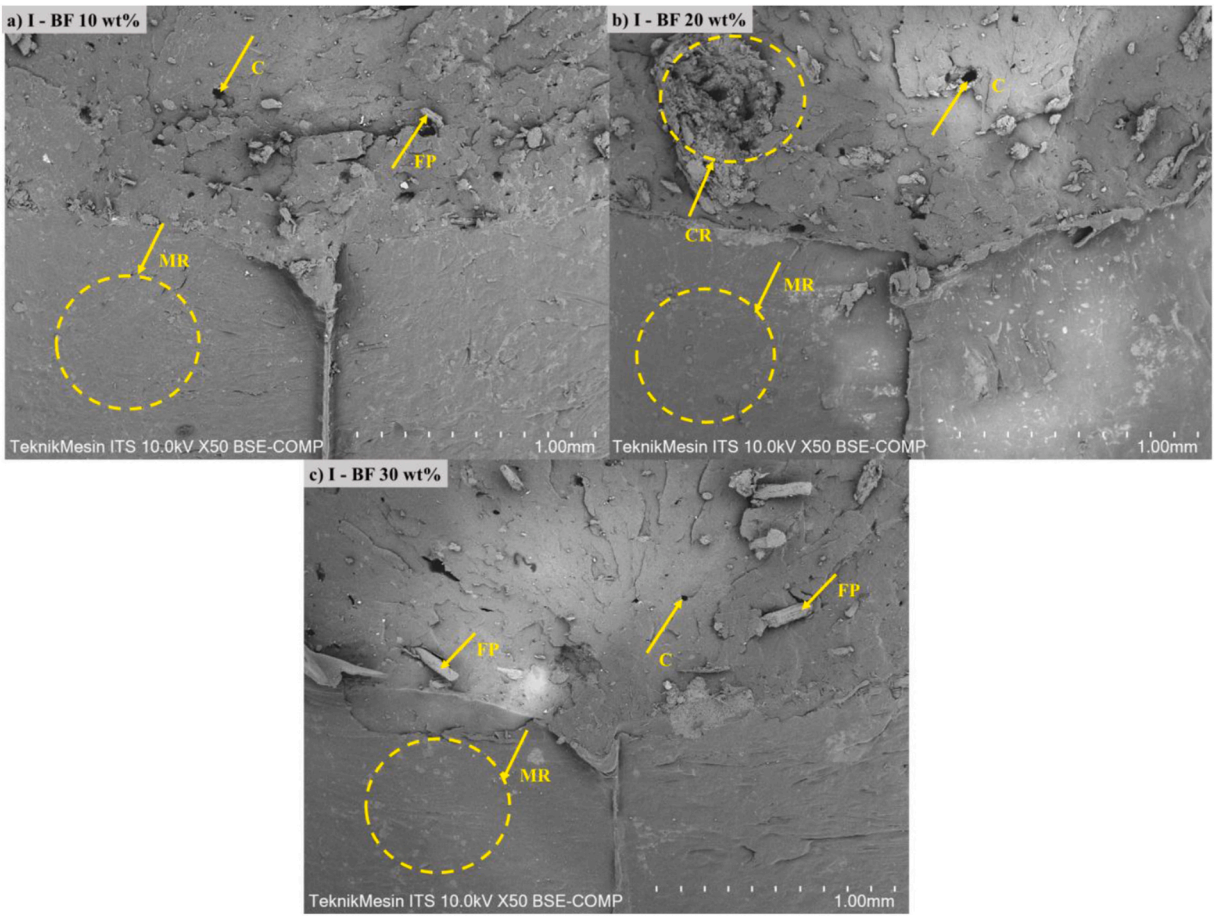

Fig. 8. SEM micrographs of the impact-fracture surfaces of PP–BF composites at fiber loadings of (a) 10 wt%, (b) 20 wt%, and (c) 30 wt%. C: localized cavity; FP: exposed fibrous particle; CR: clustered region; MR: relatively matrix-dominated region.

should not be interpreted as direct measurements of the treated, ground, and sieved particles used in this study.

Although the dimensions of the ground and sieved particles were measured before extrusion, their dimensions after extrusion and injection molding were not evaluated. Therefore, processing-induced particle attrition during melt compounding and injection molding could not be quantified. Future studies should include particle extraction from molded specimens and post-processing dimensional analysis to determine changes in particle length and aspect ratio during processing.

Comparable thermal-characterization data were not available for all three composite systems. Representative PP–coir and PP–PALF formulations had previously been examined using different thermal-analysis techniques, whereas corresponding data were not available for the PP–BF formulations. Because the three composite systems were not evaluated using an identical thermal-analysis method and testing procedure, the available information could not provide a direct comparison of their thermal behavior.

Melt-rheological characterization was also not performed. Consequently, the relative contributions of possible thermal degradation, moisture or volatile release, increased melt-flow resistance, particle agglomeration, limited matrix penetration, and interfacial effects could not be quantitatively distinguished. Therefore, the reductions in mechanical performance and morphological changes observed at higher particle loadings should be interpreted as potentially arising from a combination of these factors rather than from a single mechanism. Future studies should include comparable thermal characterization of all composite systems, FTIR analysis of untreated and treated fiber particles, post-processing particle-dimensional analysis, and melt-rheological characterization of all fiber-containing formulations.

5. Conclusions

Under identical extrusion and injection-molding conditions, fiber type and nominal loading produced distinct mechanical and fracture responses in PP biocomposites reinforced with ground low-aspect-ratio fibrous particles. PP–PALF showed the most favorable overall response, with the highest mean tensile strength of 34.91 MPa at 10 wt% and impact strength of 2.75 kJ/m^2 at 30 wt%, corresponding to numerical increases of 4.2% and 121.8%, respectively, relative to processed neat PP. Tensile strength remained relatively stable in PP–PALF but decreased at higher loadings in PP–BF and PP–CF, whereas impact strength generally increased with loading.

SEM observations revealed loading-dependent differences in matrix deformation, cavities, clustered or fiber-rich regions, exposed fibrous particles, and localized openings. These results indicate that composite performance was governed by the combined effects of particle type, loading, particle distribution, matrix continuity, interfacial interaction, and processing-induced microstructure. The study provides a controlled comparative benchmark for selecting natural-fiber type and loading in injection-molded PP biocomposites. Further work should evaluate compatibilizer content and include comparable chemical, thermal, rheological, and post-processing particle characterization.

CRediT authorship contribution statement

Arum Soesanti: Conceptualization, Investigation, Methodology, Writing – original draft. **I Made Londen Batan:** Supervision, Validation, Writing – review & editing. **Arif Wahjudi:** Conceptualization, Supervision, Writing – review & editing. **Mohammad Khoirul Effendi:** Data

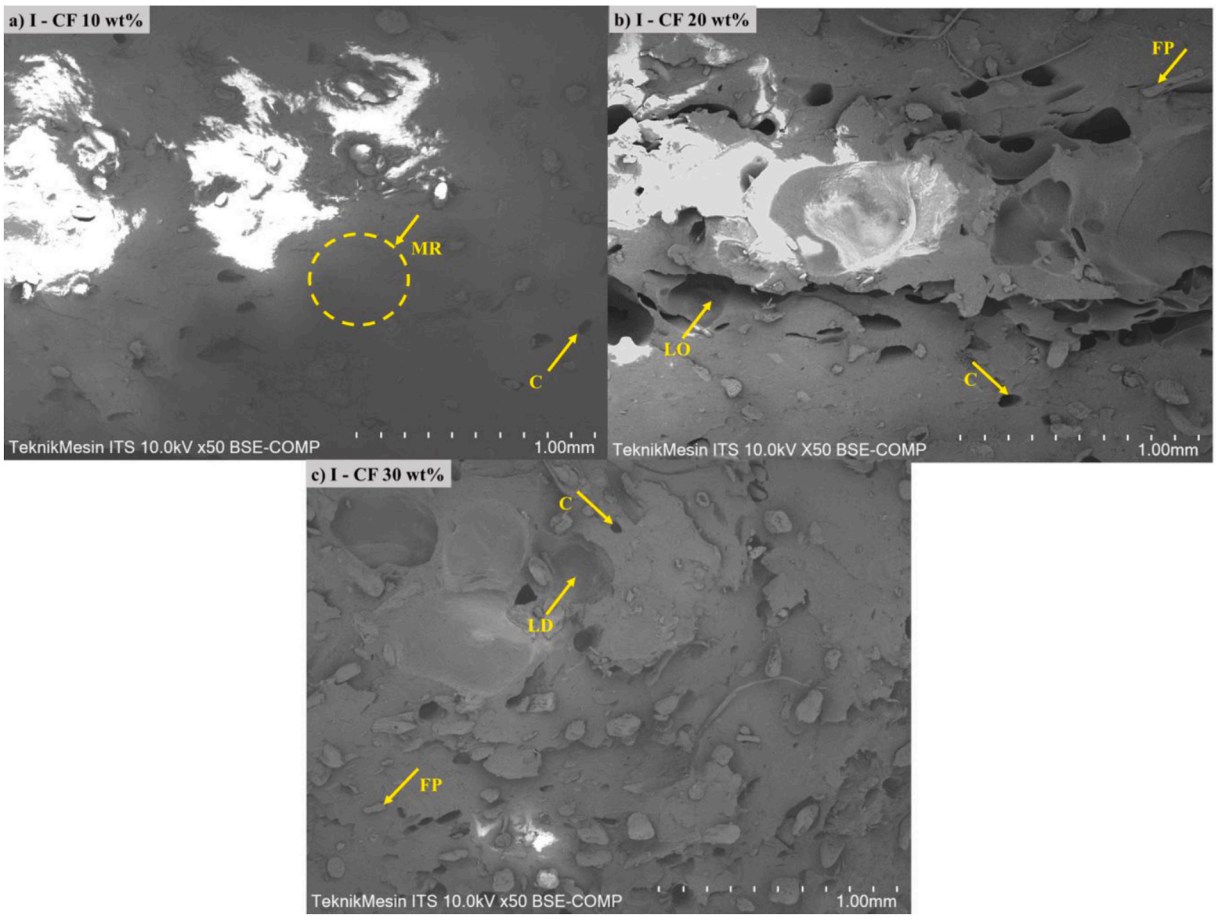

Fig. 9. SEM micrographs of the impact-fracture surfaces of PP–CF composites at fiber loadings of (a) 10 wt%, (b) 20 wt%, and (c) 30 wt%. MR: relatively matrix-dominated region; C: localized cavity; FP: exposed fibrous particle; LO: localized opening; LD: large depression.

curation, Investigation. **Maulana Yusuf Izzuddin:** Data curation, Resources. **Putu Suwarta:** Investigation, Visualization, Writing – review & editing.

Declaration of generative AI and AI-assisted technologies in the manuscript preparation process

During the preparation of this work, the authors used ChatGPT (OpenAI) to assist in the development of the manuscript outline and organization of scientific ideas. Paperpal was used for English language editing and manuscript polishing purposes. The authors critically reviewed, revised, and validated all the content and took full responsibility for the accuracy, originality, and integrity of the published work.

Funding

This research was supported by the Sepuluh Nopember Institute of Technology (ITS) through the EQUITY–World Class University (WCU) Program. Funding was provided by the Indonesian Endowment Fund for Education Agency (LPDP) under the QS Subject Ranking Scheme (Contract No. 4299/B3/DT.03.08/2025 and 3029/PKS/ITS/2025).

Declaration of competing interests

The authors declare that they have no known competing financial interests or personal relationships that could have appeared to influence the work reported in this paper.

Acknowledgment

The authors gratefully acknowledge the laboratory facilities and technical support provided by the Sepuluh Nopember Institute of Technology (ITS), which significantly contributed to the experimental work and material characterization conducted in this study. The authors also appreciate the assistance provided during the sample preparation and experimental activities.

Data availability

Data will be made available on request.

References

[1] S. Ghalme, M. Hayat, M. Harne, A comprehensive review of natural fibers: bio-based constituents for advancing sustainable materials technology, J. Renew. Mater. 13 (2) (Jan. 2025) 273–295, https://doi.org/10.32604/jrm.2024.056275.
[2] S. Palanisamy, T.M. Murugesan, M. Palaniappan, C. Santulli, N. Ayrilmis, Fostering sustainability: the environmental advantages of natural fiber composite materials – a mini review, Environ Res Technol 7 (2) (June 2024) 256–269, https://doi.org/10.35208/ert.1397380.
[3] I. Dembri, A. Belaadi, A. Lekrine, M. Jawaid, A.S. Ismail, D. Ghernaout, Effect of alkaline treatment on the thermo-physicochemical and mechanical properties of biochar powder/Washingtonia robusta fibers/PLA hybrid biocomposites, J. Mater. Res. Technol. 33 (Nov. 2024) 9735–9751, https://doi.org/10.1016/j.jmrt.2024.12.018.
[4] A. Lekrine, et al., Thermomechanical and structural analysis of green hybrid composites based on polylactic acid/biochar/treated W. filifera palm fibers, J. Mater. Res. Technol. 30 (May 2024) 9656–9667, https://doi.org/10.1016/j.jmrt.2024.06.033.
[5] S.J. Skosana, C. Khoathane, T. Malwela, Driving towards sustainability: a review of natural fiber reinforced polymer composites for eco-friendly automotive light-

weighting, J. Thermoplast. Compos. Mater. 38 (2) (Feb 2025) 754–780, https://doi.org/10.1177/08927057241254324.
[6] S. Dua, et al., Potential of natural fiber based polymeric composites for cleaner automotive component production -a comprehensive review, J. Mater. Res. Technol. 25 (June 2023) 1086–1104, https://doi.org/10.1016/j.jmrt.2023.06.019.
[7] M.S. Rabbi, T. Islam, G.M.S. Islam, Injection-molded natural fiber-reinforced polymer composites: a review, Int. J. Mech. Mater. Eng. 16 (1) (Nov. 10, 2021) 15, https://doi.org/10.1186/s40712-021-00139-1.
[8] M. Czepiel, M. Bańkosz, A. Sobczak-Kupiec, Advanced injection molding methods: review, Materials 16 (17) (Aug. 2023) 5802, https://doi.org/10.3390/ma16175802.
[9] M. Syduzzaman, M.A. Al Faruque, K. Bilisik, M. Naebe, Plant-Based natural fibre reinforced composites: a review on fabrication, properties and applications, Coatings 10 (10) (Oct. 2020) 973, https://doi.org/10.3390/coatings10100973.
[10] S. Messaoui, L. Ghali, N. Guermazi, N. Haddar, S. Msahli, Tensile properties and micromechanical modeling of polypropylene composites reinforced with alfa fibers, J. Compos. Mater. 56 (12) (Mar. 2022) 1957–1969, https://doi.org/10.1177/00219983221087482.
[11] M.A. Azman, et al., Natural fiber reinforced composite material for product design: a short review, Polymers 13 (12) (June 2021) 1917, https://doi.org/10.3390/polym13121917.
[12] J.S.S. Neto, H.F.M. De Queiroz, R.A.A. Aguiar, M.D. Banea, A review on the thermal characterisation of natural and hybrid fiber composites, Polymers 13 (24) (Dec. 2021) 4425, https://doi.org/10.3390/polym13244425.
[13] I. Elfaleh, et al., A comprehensive review of natural fibers and their composites: an eco-friendly alternative to conventional materials, Results Eng. 19 (July 2023) 101271, https://doi.org/10.1016/j.rineng.2023.101271.
[14] M. Zwawi, A review on natural fiber bio-composites, surface modifications and applications, Molecules 26 (2) (Jan. 2021) 404, https://doi.org/10.3390/molecules26020404.
[15] A. Hadou, A. Belaadi, M. Boumaaza, B.X. Chai, I.M.H. Alshaikh, D. Ghernaout, Developing and characterizing Dracaena draco fiber-reinforced bio-epoxy composites for sustainable structural applications, Results Eng. 29 (Mar. 2026) 108444, https://doi.org/10.1016/j.rineng.2025.108444.
[16] O. Ferfari, A. Belaadi, B.X. Chai, D. Ghernaout, Enhancing bio-epoxy composites with Syagrus romanzoffiana palm fibers: impact of fiber loading on thermomechanical and water absorption properties, Ind. Crop. Prod. 238 (Dec. 2025) 122384, https://doi.org/10.1016/j.indcrop.2025.122384.
[17] V. Mahesh, R. Gobinath, M.S. Kırgız, R.P.V. Shekar, M. Shewale, Global trends of research productivity in natural fibre reinforced composites: comprehensive scientometric analysis, J. Nat. Fibers 19 (16) (June 2022) 13088–13105, https://doi.org/10.1080/15440478.2022.2085227.
[18] T. Höftberger, G. Zitzenbacher, C. Burgstaller, Influence of processing parameters in injection molding on the properties of short carbon and glass fiber reinforced polypropylene composites, Polymers 16 (19) (Sept. 2024) 2745, https://doi.org/10.3390/polym16192745.
[19] A. Lekrine, A. Belaadi, I. Dembri, M. Jawaid, A.S. Ismail, D. Ghernaout, Fiber treatment impact on the thermal behavior of biomass/palm-fibers polylactic-acid hybrid biocomposites, Mater. Chem. Phys. 338 (July 2025) 130651, https://doi.org/10.1016/j.matchemphys.2025.130651.
[20] I. Dembri, et al., Structural and thermal properties of Alkali-treated biomass fibers and W. robusta waste reinforced PLA hybrid biocomposites, Case Stud. Therm. Eng. 70 (June 2025) 106170, https://doi.org/10.1016/j.csite.2025.106170.
[21] J.B. Dawit, Y. Regassa, H.G. Lemu, Property characterization of acacia tortilis for natural fiber reinforced polymer composite, Results Mater. 5 (Mar. 2020) 100054, https://doi.org/10.1016/j.rinma.2019.100054.
[22] M. Asim, K. Abdan, M. Jawaid, M. Nasir, Z. Dashtizadeh, M.R. Ishak, M.E. Hoque, A review on pineapple leaves fibre and its composites, Int. J. Polym. Sci. 2015 (2015) 950567, https://doi.org/10.1155/2015/950567.
[23] A. Pappu, V. Patil, S. Jain, A. Mahindrakar, R. Haque, V.K. Thakur, Advances in industrial prospective of cellulosic macromolecules enriched banana biofibre resources: a review, Int. J. Biol. Macromol. 79 (2015) 449–458, https://doi.org/10.1016/j.ijbiomac.2015.05.013.
[24] A.G. Adeniyi, D.V. Onifade, J.O. Ighalo, A.S. Adeoye, A review of coir fiber reinforced polymer composites, Compos. B Eng. 176 (Aug. 2019) 107305, https://doi.org/10.1016/j.compositesb.2019.107305.
[25] L. Jiang, Y. Zhou, F. Jin, Design of short fiber-reinforced thermoplastic composites: a review, Polym. Compos. 43 (8) (June 2022) 4835–4847, https://doi.org/10.1002/pc.26817.
[26] A. Ramachandran, S. Mavinkere Rangappa, V. Kushvaha, A. Khan, S. Seingchin, H. N. Dhakal, Modification of fibers and matrices in natural fiber reinforced polymer composites: a comprehensive review, Macromol. Rapid Commun. 43 (17) (June 2022) 2100862, https://doi.org/10.1002/marc.202100862.
[27] M. Akter, M.H. Uddin, I.S. Tania, Biocomposites based on natural fibers and polymers: a review on properties and potential applications, J. Reinforc. Plast. Compos. 41 (17–18) (Feb. 2022) 705–742, https://doi.org/10.1177/07316844211070609.
[28] S.M. Rangappa, S. Siengchin, J. Parameswaranpillai, M. Jawaid, T. Ozbakkaloglu, Lignocellulosic fiber reinforced composites: progress, performance, properties, applications, and future perspectives, Polym. Compos. 43 (2) (Nov. 2021) 645–691, https://doi.org/10.1002/pc.26413.
[29] T. Nampitch, Mechanical, thermal and morphological properties of polylactic acid/natural rubber/bagasse fiber composite foams, Results Mater. 12 (Sept. 2021) 100225, https://doi.org/10.1016/j.rinma.2021.100225.
[30] J.I.P. Singh, S. Singh, V. Dhawan, Influence of fiber volume fraction and curing temperature on mechanical properties of jute/PLA green composites, Polym. Polym. Compos. 28 (4) (Sept. 2020) 273–284, https://doi.org/10.1177/0967391119872875.
[31] F. Seculi, F.X. Espinach, R.J. Aguado, P. Mutjé, Q. Tarrés, Simple model to predict the intrinsic flexural modulus of abaca strands from crystallinity and microfibril angle, Polym. Compos. 46 (5) (Nov. 2025) 4558–4575, https://doi.org/10.1002/pc.29259.
[32] T. Khuntia, S. Biswas, An investigation on the flammability and dynamic mechanical behavior of coir fibers reinforced polymer composites, J. Ind. Textil. 51 (10) (Feb. 2022) 1616–1640, https://doi.org/10.1177/1528083720905031.
[33] M.E. Vallejos, et al., Response of polypropylene composites reinforced with natural fibers: impact strength and water-uptake behaviors, Polymers 15 (4) (Feb. 2023) 900, https://doi.org/10.3390/polym15040900.
[34] H.T.N. Kuan, M.Y. Tan, Y. Shen, M.Y. Yahya, Mechanical properties of particulate organic natural filler-reinforced polymer composite: a review, Compos. Adv. Mater. 30 (Jan. 2021) 263498332110075, https://doi.org/10.1177/26349833211007502.
[35] K. Nasri, É. Loranger, L. Toubal, Effect of cellulose and lignin content on the mechanical properties and drop-weight impact damage of injection-molded polypropylene-flax and -pine fiber composites, J. Compos. Mater. 57 (21) (June 2023) 3347–3364, https://doi.org/10.1177/00219983231186208.
[36] N. Sultana, et al., Short jute fiber preform reinforced polypropylene thermoplastic composite: experimental investigation and its theoretical stiffness prediction, ACS Omega 8 (27) (June 2023) 24311–24322, https://doi.org/10.1021/acsomega.3c01533.
[37] S.R. Gorrepotu, K. Debnath, R.N. Mahapatra, T.S. Srivatsan, A critical review on mechanical and morphological characteristics of injection molded biodegradable composites, Polym. Compos. 43 (12) (Oct. 2022) 8634–8672, https://doi.org/10.1002/pc.27096.
[38] M.A.H. Shibly, et al., Characteristic evaluation of polypropylene matrix composite reinforced with Corypha taliera fruit fibers, Results Mater. 27 (Sept. 2025) 100744, https://doi.org/10.1016/j.rinma.2025.100744.
[39] R. Naghdi, T. Nejat, Effects of organically-modified montmorillonite and alkalinization on physical, mechanical, chemical, morphological, and thermal properties of wheat straw/recycled polypropylene nanocomposites, J. Compos. Mater. 57 (13) (Apr. 2023) 2127–2144, https://doi.org/10.1177/00219983231168946.
[40] E. Gürpınar, C.H. Ünlü, A review of plant derived biomass particulate-reinforced thermoplastic polymer composites and their mechanical characteristics, Compos. Commun. 64 (Mar. 2026) 102786, https://doi.org/10.1016/j.coco.2026.102786.
[41] H. Taghipoor, S. Ghorbani, Experimental investigation of low-velocity impact response in PP/date palm fiber bio-composites reinforced with compatibilizer and impact modifier, Mater. Today Commun. 51 (Feb. 2026) 114771, https://doi.org/10.1016/j.mtcomm.2026.114771.
[42] I. Lalaymia, A. Belaadi, B.X. Chai, D. Ghernaout, Structural and thermomechanical characterization of a new bio-epoxy composite reinforced with agave waste flower stalk fibers for sustainable applications, Ind. Crop. Prod. 241 (Mar. 2026) 122800, https://doi.org/10.1016/j.indcrop.2026.122800.
[43] M. Abdullah, S. Saha, M.S.H. Motayed, M.H. Ali, M.A. Habib, Banana and bamboo filler-reinforced epoxy resin composites: analysis of mechanical and physical properties, Results Eng. 28 (Dec. 2025) 107293, https://doi.org/10.1016/j.rineng.2025.107293.
[44] A.A. Aliu, et al., Sustainable hybrid composite ceiling tiles from waste LDPE reinforced with Sida acuta fibers and recycled paper pulp nanofillers: mechanical, thermal and microstructural performance, Results Eng. 30 (June 2026) 110302, https://doi.org/10.1016/j.rineng.2026.110302.
[45] S. Kyatanavar, et al., Enhancing mechanical and thermal properties of jute-banana-phenol formaldehyde hybrid composites using Bio waste fillers: experimental Study and ANN prediction, J. Nat. Fibers 23 (1) (Jan. 2026) 2617369, https://doi.org/10.1080/15440478.2026.2617369.